STATIONKEEPING AND SLEWING CONTROL OF A MULTI-TETHERED AEROSTAT

Gabriele Gilardi and Meyer Nahon

Department of Mechanical Engineering, McGill University
Montreal, Quebec, Canada, H3A 2K6
Meyer.Nahon@mcgill.ca

Abstract: This paper discusses two control issues in a novel design of radio telescope. The receiver of the telescope is held aloft by an aerostat and tethered to the ground by a number of cables, each controlled by a winch to allow positioning of the receiver. This paper discusses the gain optimization for stationkeeping control and compares approaches for slewing the receiver through gross motions. *Copyright © 2004 IFAC*

Keywords: Telescopes, Cables, Dynamics, Mechanisms, PID Control, Optimization

1. INTRODUTION

Radio astronomers from around the world have recently advocated the need for a new radio telescope with a collecting area of 10^6 m^2 which is dubbed the Square Kilometer Array (SKA) (van de Weygaert and van Albada, 1996). A conceptual design from the National Research Council of Canada's Herzberg Institute of Astrophysics consists of an array of about 50 very large antennas. The novel antenna design, depicted in Figure 1, is called the Large Adaptive Reflector (LAR) (Fitzsimmons, *et al*., 2000). The LAR design includes two central components. The first is a 200 m diameter parabolic reflector, with a focal length of 500 m, composed of actuated panels, mounted on the ground. The second is a focal package held aloft at a height of 500 meters by a large helium balloon (aerostat) and a system of three or more taut tethers. This tension structure is large enough that it filters out all but the lowest frequency turbulence, and stiff enough that it effectively resists wind forces. The telescope is steered by modifying the shape of the reflector, and simultaneously changing the lengths of the tethers with winches so that the receiver is positioned on the surface of a hemisphere of radius 500 m, centered at the reflector. The variable-length tethers also allow some measure of control of the receiver position in response to disturbances such as wind gusts (Fitzsimmons, *et al*., 2000; Nahon, *et al*., 2002).

A one-third scale prototype of the multi-tethered aerostat subsystem for LAR has been constructed as a proof of concept for this design (Lambert, *et al*., 2003). In parallel, a computer simulation has been developed. The simulation can be used to weigh alternative design options, determine how typical gusts are likely to affect the receiver positioning accuracy, and perform preliminary evaluation of the winch control algorithms.

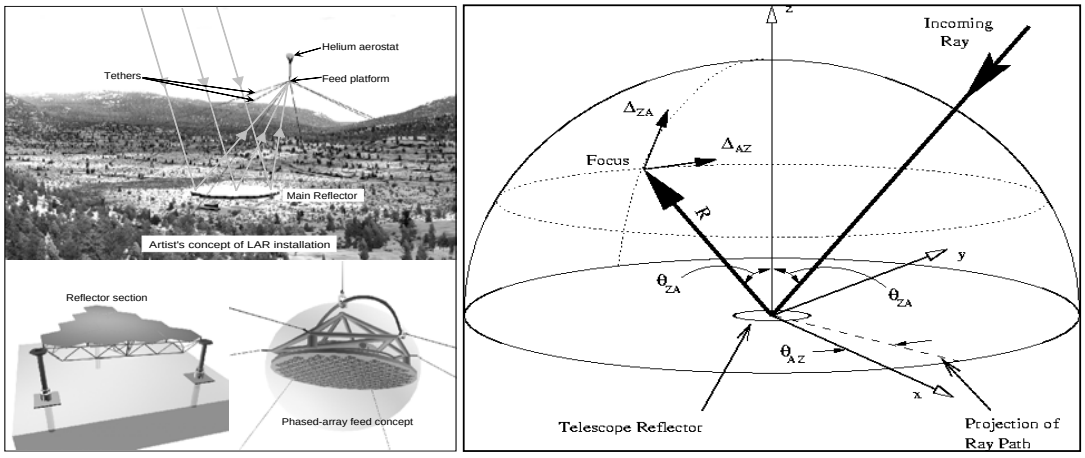

Fig. 1. LAR Design Concept.

Most literature on tethered aerostat systems has considered the open-loop (uncontrolled) behaviour of a streamlined aerostat held down by a single tether. Some prior work at the National Research Council of Canada dealt with the static or steady-state performance of a triple-tethered aerostat system (Fitzsimmons, *et al*., 2000). Another interesting study is an experiment conducted by the US Air Force on the dynamic behavior of a tri-tethered aerostat (Leclaire and Rice, 1973).

This paper discusses some control issues in the LAR tethered aerostat system. Two types of controlled maneuvers are required with this system: *stationkeeping*, i.e. prescribing a fixed position for the payload, and *slewing*, i.e. moving the payload from one point to another. In the case of stationkeeping, the gain optimization methodology is discussed. In the case of slewing, the paper compares various methods for accomplishing such large scale motion. Numerical results are presented to show the effectiveness of the proposed approaches.

2. SYSTEM MODEL

The dynamics model of this multi-tethered aerostat system has been discussed extensively elsewhere, but is briefly reviewed here. Figure 2 shows a layout of the system, which includes an aerostat, a confluence point where all tethers meet and the payload (receiver) is located, a leash (the single cable connecting the aerostat to the confluence point), three to six tethers connecting the confluence point to the ground, and winches at the base of each tether.

The aerostat may be spherical or streamlined. The spherical aerostat is modeled as a sphere whose drag varies with Reynolds number (Nahon, *et al*., 2002). Modeling of the streamlined aerostat is more involved and is discussed in (Lambert and Nahon, 2003)---a component breakdown approach is used to model the aerodynamic behavior of the hull and each fin. These are then summed to find the overall behavior of the aerostat. The confluence point is modeled as a sphere, similarly to the spherical aerostat (Nahon, *et al*., 2002).

The cable is discretized into elements and the mass of each element is lumped at its endpoints (Lambert and Nahon, 2003). The equations of motion for each lumped mass are then formulated, including the internal forces (stiffness, damping) and external forces (aerodynamic, weight).

The entire system of second-order nonlinear dynamics equations is assembled, put into first order form, and then solved using a fourth-order Runge-Kutta integration routine (Press, *et al*., 1992).

The disturbances to the system are due to the turbulent wind. This is modeled using a mean wind varying with height, due to the earth's planetary boundary layer. Superimposed on this, are turbulent gusts with a von Karman spectrum. Further details given in (Nahon, *et al*., 2002).

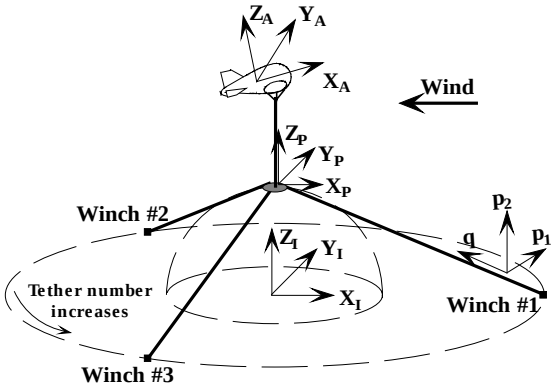

Fig. 2. System Layout.

3. STATIONKEEPING

The closed-loop stationkeeping controller uses feedback of the measured payload position to alter the length of the tethers, thus compensating for wind disturbances. The error signal for each tether is evaluated as

$$e_i = \left\|\mathbf{p}(t) - \mathbf{p}_{Wi}\right\| - \left\|\mathbf{p}_d(t) - \mathbf{p}_{Wi}\right\| \qquad (1)$$

where $\mathbf{p}_d$ is the desired payload position, $\mathbf{p}$ is the actual location, and $\mathbf{p}_{Wi}$ is the winch position. The motivation behind this approach is that, if the distance from each winch to the payload is correct, then the payload lies on a sphere of radius $\left\|\mathbf{p}_d - \mathbf{p}_{Wi}\right\|$ centered at the winch. If all the payload-winch distances are correct, then the payload lies at the intersection of those spheres which defines the correct desired location of the payload in 3-D space. Using a PID control law, the change in tether length needed to minimize e_i can be written as

$$\Delta L_i = -\left(k_P e_i + k_D \dot{e}_i + k_I \int e_i dt\right) \qquad (2)$$

or, in terms of velocity as

$$\dot{L}_i = -\left(k_P \dot{e}_i + k_D \ddot{e}_i + k_I e_i\right) \qquad (3)$$

where k_P, k_D, k_I are, respectively, the proportional, derivative and integral gains. The three gains are the same for all tethers, as no advantage was found for them to be different. For practical reasons, the PID defined has been implemented in its derivative form, equation (3), i.e. on the tether speed. The change in the tether length is then determined as integral of the tether speed.

3.1 Gain Optimization

A procedure to optimize the PID gains has been developed. The total error is first defined as

$$\mathbf{e} = \mathbf{p} - \mathbf{p}_d \qquad (4)$$

where **p** is the actual payload position and $\mathbf{p}_d$ is the desired payload position. It is useful to make a distinction between the components of this vector in and out of the focal plane. The focal plane is defined as the local tangent plane to the focal hemisphere, at the given zenith and azimuth angles. If **e** is expressed in the inertial frame, then the components in the focal plane, e_{f1} and e_{f2}, and out of the focal plane, e_{of}, are given by

$$\begin{Bmatrix} e_{f1} \\ e_{f2} \\ e_{of} \end{Bmatrix} = \begin{bmatrix} \cos\theta_{AZ}\cos\theta_{ZA} & \sin\theta_{AZ}\cos\theta_{ZA} & -\sin\theta_{ZA} \\ -\sin\theta_{AZ} & \cos\theta_{AZ} & 0 \\ \cos\theta_{AZ}\sin\theta_{ZA} & \sin\theta_{AZ}\sin\theta_{ZA} & \cos\theta_{ZA} \end{bmatrix} \cdot \mathbf{e} \tag{5}$$

where θ_{AZ} and θ_{ZA} are, respectively, the azimuth and the zenith angles (Figure 1). We define the error in the focal plane as

$$e_f = \sqrt{e_{f1}^2 + e_{f2}^2} \tag{6}$$

The objective function we wish to minimize is

$$f = \int_0^{t_f} \left(w_f \left\| e_f \right\| + w_{of} \left\| e_{of} \right\| \right) dt \tag{7}$$

where w_f and w_{of} are the corresponding weights, and the integral is evaluated between zero and the final time t_f. Thus, we are minimizing a weighted sum of the components of the total error over a simulation of duration t_f. The integral in (7) is computed using a trapezoidal rule (Press, *et al*., 1992).

We impose the following constraints on the gains to ensure their magnitudes remain reasonable

$$k_{\min} \le k_i \le k_{\max} \qquad i = P, D, I \tag{8}$$

where k_{min} and k_{max} are the lower and upper bounds, respectively. These constraints are imposed using a penalty function of the form

$$\Phi_i = \left(\min\left[0, k_i - k_{\min}\right]\right)^2 + \left(\max\left[0, k_i - k_{\max}\right]\right)^2 \tag{9}$$

where $i = P, D, I$. Similarly, a bound is imposed on the maximum power needed at any one winch, i.e.,

$$\Phi_P = \left(\max\left[0, \max(P_i) - P_{\max}\right]\right)^2 \tag{10}$$

where P_{max} is the upper bound. Finally, if the system becomes unstable at time t because of the gains, another penalty function is added, in the form

$$\Phi_u = \left(t - t_f\right)^2 \tag{11}$$

Thus, the function used for the optimization is

$$f = \int_0^{t_f} \left(w_f \left\| e_f \right\| + w_{of} \left\| e_{of} \right\| \right) dt + \sum_{i=P,D,I} \Phi_i + \Phi_p + \Phi_u \tag{12}$$

Powell's method (Press, *et al*., 1992) was used to perform the optimization. The dynamics simulation was embedded within the optimizer to allow the objective function to be evaluated. At each iteration of the optimizer, a simulation was run to evaluate (12). Depending on the results, the optimizer would adjust the gains, until eventually an optimal set of gains was found.

3.2 Numerical Results

Before proceeding with the optimization, we first performed a sensitivity study to see how the maximum total error and the maximum (positive) power vary with the main parameters, i.e. zenith angle, azimuth angle, wind speed and wind direction (the error considered here is the total error, defined in (4)). The system considered consisted of a full scale tri-tether configuration with a streamlined aerostat, constant wind (but with different values), turbulence and PID gains of k_P = 5, k_D = 3, k_I = 1. Simulations were run for t_f = 100 seconds.

Table 1 shows the maximum error and power changing the wind speed, keeping fixed the other parameters (zenith and azimuth angles equal to zero and wind direction equal to 180°). As expected, both increase monotonically as the wind speed increases.

Table 1. Error & Power Variation with Wind Speed

Wind speed [m/s]	Max. error [cm]	Max. power [kW]
0	0	0
2	2.2	0.42
4	7.2	1.89
6	13.0	6.35
8	29.8	10.69
10	43.7	20.03

Table 2 shows the maximum error and power with changes in the zenith angle, keeping the other parameters fixed (azimuth angle at zero, wind speed at 10 m/s and wind direction of 180°). While the power increases monotonically with the zenith angle, the progression of the error is less clear.

Table 2. Error & Power Variation with Zenith Angle

Zenith [°]	Max. error [cm]	Max. power [kW]
0	43.7	20.03
10	46.8	22.07
20	48.8	23.63
30	45.7	26.26
40	49.8	28.31
50	53.0	33.39
60	75.9	36.98

Figure 3 shows a plot of the maximum error and the maximum power for different azimuth angles and wind directions. The other two parameters were kept constant at their worst case values (wind speed of 10 m/s and zenith angle of 60°). In the plot, each curve has been shifted by an angle equal to the corresponding azimuth angle, to show that the shapes are quite similar. Thus, the actual wind direction for the curve with azimuth θ_{AZ} is given by the wind direction in the plot plus θ_{AZ}. For the power this similarity is less well defined.

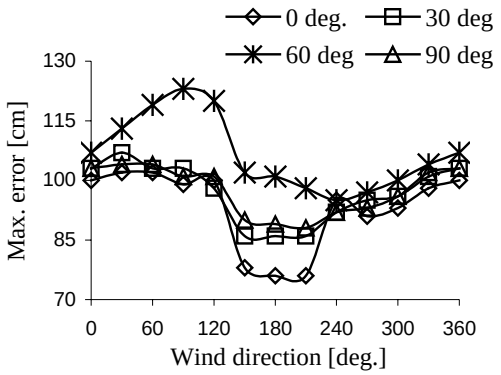

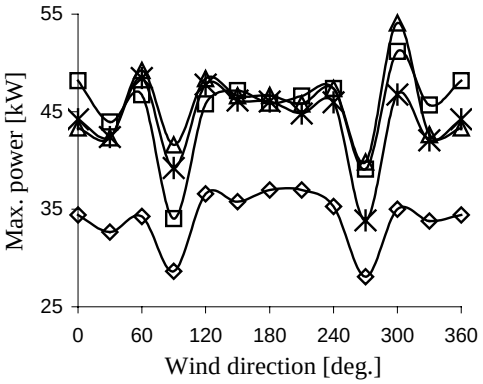

Fig. 3. Effect of Azimuth and Wind Direction

The worst configuration in term of maximum error was at 60° in zenith and azimuth, 10 m/s wind speed and 150° wind direction. Using this configuration, we performed a gain optimization, starting from gain values of $k_P = 5$, $k_D = 3$, $k_I = 1$. Constraints of $k_{min} = 0$ and $k_{max} = 10$, and $P_{max} = 75$ kW were used. For the errors in and out of the focal plane, weights of $w_f = w_{of} = 0.1$ were used.

Figure 4 shows a comparison of the total error with the optimal gains of $k_P = 9.9$, $k_D = 10$, $k_I = 8.1$ and with the unoptimized gains of $k_P = 5$, $k_D = 3$, $k_I = 1$. The maximum winch power with the optimized gains was found to be 71.2 kW. As can be seen, the optimization of the gains results in a significant decrease of the errors in payload motion.

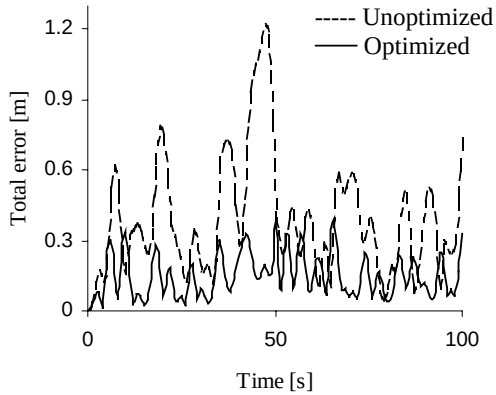

Fig. 4. Comparison of Payload Errors

4. SLEWING CONTROL

Slewing refers to the gross motion of the payload from one point to another. This is done in order to observe a different location in the sky, i.e., the incoming ray in Figure 1 is to be rotated to another location. When this is done, the reflector's curvature is changed to have a different focus, but one which remains on the surface of a virtual hemisphere of 500 m diameter, centered at the center of the reflector. The receiver (payload) must correspondingly be moved to that focus. It is important for slewing maneuvers to be accomplished quickly since any time spent slewing reduces observation time.

4.1 Trajectory

To move the desired payload position between two points, two different trajectories were considered (see Figure 5). The lower part of the figure is the section along axis **u**.

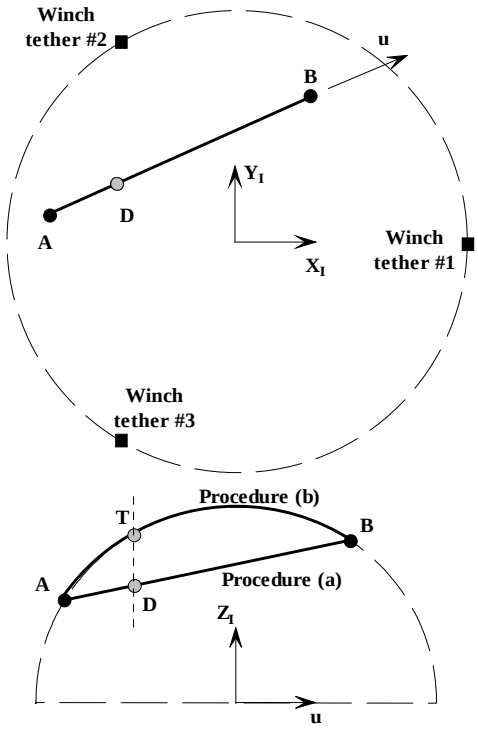

Fig. 5. Slewing Trajectories

In procedure (a) the desired payload position is moved from point A to point B along the shortest path possible, i.e. a straight line connecting the two points. The coordinates of points A, (x_A, y_A, z_A), and B, (x_B, y_B, z_B), can be found from the corresponding focal length, zenith and azimuth angles (Figure 1),

$$\begin{aligned} x_i &= R\cos\theta_{AZ}\sin\theta_{ZA} \\ y_i &= R\sin\theta_{AZ}\sin\theta_{ZA} \\ z_i &= R\cos\theta_{ZA} \end{aligned} \qquad i = A, B \qquad (13)$$

The generic position along this line, point D, is then found using

$$\begin{aligned} x_d &= f(x_B - x_A) \\ y_d &= f(y_B - y_A) \\ z_d &= f(z_B - z_A) \end{aligned} \tag{14}$$

where f is a function representing the time-profile (linear or sinusoidal ramp) used for the maneuver. Finally, the spherical co-ordinates for point D at each instant during the maneuver can be found from

$$\begin{aligned} r &= \sqrt{x_d^2 + y_d^2 + z_d^2} \\ \theta_{ZA} &= \cos^{-1}(z_d / r) \\ \theta_{AZ} &= \tan^{-1}(y_d / x_d) \end{aligned} \tag{15}$$

In procedure (b), the desired payload position is moved on a trajectory on the surface of the virtual hemisphere between A and B. This path is obtained by projecting the straight line between A and B vertically onto the hemisphere defined by the focal length R. The position along this line, point T, is obtained using the original point D as shown in Figure 5. Its coordinates are defined by (x_d, y_d, z_t), with z_t given by

$$z_t = \sqrt{R - (x_d^2 + y_d^2)} \tag{16}$$

It should be noted that these two procedures just change the *desired* payload position, but not the actual payload position. To force the payload to follow the change in the desired payload position, a controller must be used. The control may be open-loop or closed-loop. In each case the tether lengths are changed to keep the actual payload position as close as possible to the desired position.

4.2 Open-Loop Slewing

The open-loop controller works by changing the length of the tethers to follow the change in the payload's desired position, without using any feedback on the actual payload position. Figure 6 shows the scheme used.

Using one of the two procedures illustrated in the previous section, the desired payload position is changed from $\mathbf{p}_d(t_0)$ to $\mathbf{p}_d(t_0+\Delta t)$ with a known function of time. The change in the i^{th} tether length is assumed to be

$$\Delta L_i = k_{Pi}\left(\left\|\mathbf{p}_d(t_0 + \Delta t) - \mathbf{p}_{Wi}\right\| - \left\|\mathbf{p}_d(t_0) - \mathbf{p}_{Wi}\right\|\right) \tag{17}$$

If the angle α is small (i.e. the winch is far from the payload and/or the time Δt is small), this is a good approximation. Note that when the desired payload position reaches point B, the tether stops changing its length, but the length at that time is not necessarily the length corresponding to a static analysis at point B. This means that the payload will not be exactly at the point B, but close to it. Usually the error in the final payload position was found to be less than 1%. The gain k_P, usually equal to 1, can be used to reduce this error.

A second method for open-loop control of the system is to directly change the length of each tether.

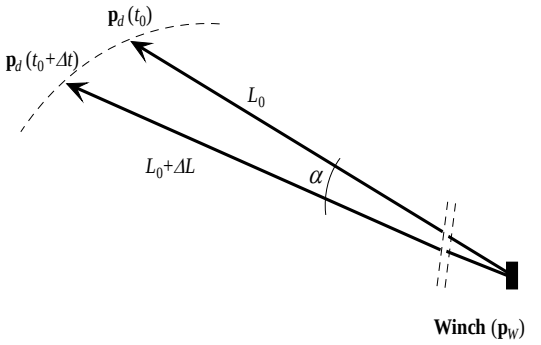

Fig. 6. Open Loop Slewing

For the i^{th} tether, if L_{Ai} and L_{Bi} are the tether lengths when the payload is in positions A and B, respectively, the function applied is

$$\Delta L_i = f(L_{Bi} - L_{Ai}) \tag{18}$$

where, again f denotes the time profile. In this case if the tether lengths corresponding to the static position of points A and B are known exactly, then the final position will be reached exactly.

4.3 Open-Loop Slewing Results

In this Section, we compare the open-loop slewing results with different control approaches. In all cases, the full scale tri-tethered configuration and the streamlined aerostat have been used. Note that in the following plots the positions are actual positions and not referred to the initial static position.

The first example is an open-loop slewing between three points. Positions and corresponding tether lengths in the static configurations are:

Table 3. Tether Lengths in Different Configurations

Point (Zenith/Azimuth)	L_1 [m]	L_2 [m]	L_3 [m]
A (60°/60°)	1076.21	1076.21	1652.46
B (30°/-130°)	1438.68	1374.06	1045.37
C (0/0)	1297.64	1297.64	1297.64

Slewing between points A and B was performed using a sinusoidal ramp, between 0 and 750 seconds. After 50 seconds a second slewing was performed between points B and C, again using a sinusoidal ramp over 750 seconds. No wind or turbulence was present. The first type of open loop controller was used (equation (17)), with all the gains equal to 1. First, the two trajectories illustrated in Figure 5 were compared, i.e. moving the payload along the shortest path and moving the payload along the circular path. Small to moderate differences were present in the tether length, speed and tension. Of course the z-position for the payload was different, while positions in x and y were basically the same. The maximum power in the first trajectory was found to be 46.0 kW, while in the second case it was 35.7 kW. As explained in Section 4.2, due to the approach used to calculate the length changes, the actual tethers length at points B and C do not correspond to the values found with a static analysis at those

points. The actual lengths were all within 0.3% of the correct lengths, and this resulted in a position error of about 5 m at the target locations.

The same maneuver was also performed with a 10 m/s wind. It was found that the wind tended to damp the aerostat oscillations. The time used to complete the maneuver also has a great influence on the results. The longer this time, the less power is required and the fewer oscillations occur.

The next example is the same maneuver (from point A to B then to C), but performed using the second type of open-loop controller, i.e. directly changing the length of the tethers (equation 18). The variations in length are:

Table 4. Length Changes for Open-Loop Slewing

Point (Zenith/Azimuth)	ΔL_1 [m]	ΔL_2 [m]	ΔL_3 [m]
A (60°/60°)			
B (30°/-130°)	+362.47	+297.85	-607.09
C (0/0)	-141.04	-76.42	+252.27

These length changes were used with the same time profile used to move the payload with the first controller. Results were compared to open-loop slewing with equation (17) and trajectory (a), used in the previous example. The differences were found to be relatively minor---some minor oscillations in tether tensions were observed with equation (18), but this controller brought the system closer to the desired configuration than did the controller with equation (17).

4.4 Closed-Loop Slewing

A closed-loop slewing maneuver can be achieved by changing the desired payload position and using the PID control law given by equation (1). The same maneuver used in Section 4.3 with trajectory (a) was considered. We compared the closed loop controller with gains of $k_P = 5$, $k_D = 3$, $k_I = 1$, to the first open-loop controller. Results were generally similar, and the maximum power was 46.2 kW. Significant differences were found in the total error (Figure 7).

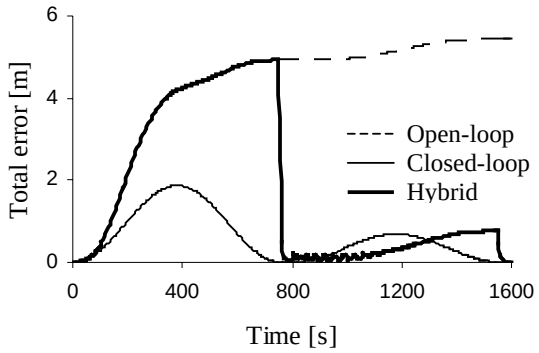

Fig. 7. Open-Loop, Closed-Loop & Hybrid Slewing

When the two maneuvers are finished, the closed-loop controller brings the system closer to the desired configuration than the open loop controller.

Considering the preceding results, and noting that tracking a particular payload trajectory is not usually crucial during a slewing maneuver, a hybrid of the two methods is also shown. Here, the slewing maneuver is performed in open loop, a PID is then activated at $750 < t < 800$ s and $t > 1550$ s (the PID gains are activated using a sinusoidal ramp of 5 seconds). Figure 7 shows the corresponding error. The hybrid controller allows the error to return to zero at the target points but allows larger error during slewing. Because the large-scale slewing is done in open-loop, the chance of encountering instabilities is much reduced.

5. CONCLUSION

This paper discussed two issues related to the control of a novel design of radio telescope: the optimization of stationkeeping control gains, and slewing control. A gradient descent scheme was used to find optimal gains for the stationkeeping controller, and these resulted in substantially better performance than with the unoptimized gains.

For slewing control, it was found that a curvilinear trajectory between the two target points resulted in lower power required. Furthermore, good results were obtained using an open-loop controller during the slewing, and then activating a closed-loop controller on reaching the target point.

REFERENCES

Fitzsimmons, J.T., B. Veidt and P. Dewdney (2000). Steady-State Stability Analysis of the Multi-Tethered Aerostat Platform for the Large Adaptive Reflector Telescope. *Proceedings of SPIE*, **4015**, 476-487.

Lambert, C. and M. Nahon (2003). Stability Analysis of a Tethered Aerostat. *AIAA Journal of Aircraft*, **40**, 705-715.

Lambert, C., A. Saunders, C. Crawford and M. Nahon (2003). Design of a One-Third Scale Multi-Tethered Aerostat System for Precise Positioning of a Radio Telescope Receiver. *CASI Flight Mechanics and Operations Symposium*, Montreal, Canada.

Leclaire, R.C. and C.B. Rice (1973). The Local Motions of a Payload Supported by a Tri-tethered Natural Shape Balloon. *US Air Force Report*, AFCRL-TR-73-0748.

Nahon, M., G. Gilardi and C. Lambert (2002). Dynamics and Control of a Radio Telescope Receiver Supported by a Tethered Aerostat. *AIAA Journal of Guidance, Control and Dynamics*, **25**, 1107-1115.

Press, W.H., S.A. Teukolsky, W.T. Vetterling and B.P. Flannery (1992). *Numerical Recipes in C: The Art of Scientific Computing*, Cambridge University Press, New York.

van de Weygaert, R. and T. S. van Albada (1996), New Challenges for Cosmology. *The Westerbork Observatory, Continuing Adventure in Radio Astronomy*, Astrophysics and Space Science Library, **207**, 225-259.